Journal of Mineralogical and Petrological Sciences, Volume 98, page 167-180, 2003

Effect of temperature and pressure on the crystal structure of topaz, $Al_2SiO_4(OH,F)_2$

Kazuki KOMATSU*, Takahiro KURIBAYASHI* and Yasuhiro KUDOH*

**Institute of Mineralogy, Petrology, and Economic Geology, Faculty of Science, Tohoku University, Sendai 980-8578, Japan*

The effect of temperature and pressure was analyzed on the crystal structure of natural topaz from Gilgit division, Pakistan. The unit cell parameters at 298K, 423K, 573K, 723K, 873K, 1023K and 1173K, and X-ray diffraction intensity data at 298K, 573K, 873K and 1173K were collected using an imaging plate X-ray diffractometer equipped with rotating anode generator. Thermal expansion coefficients along the unit cell edges and of the volume are α_a=6.4(7)×10^{-6}K^{-1}, α_b=5.5(6) ×10^{-6}K^{-1}, α_c=8.1(6) ×10^{-6}K^{-1} and α_V =2.0(1) ×10^{-5}K^{-1}. The results of structure refinement taking into account the anisotropic displacement parameters at these temperatures yielded *R* values of 2.48, 2.60, 2.56 and 2.70%. The increase of mean Al-O distance with temperature was greater than those of Al-F and Si-O. The Al-F-Al bond angle decreased with the increase of displacement parameter of fluorine-atom. The unit cell parameters under pressures up to 6.8 GPa and X-ray diffraction intensity data under 0.0001(ambient pressure), 3.7, 5.1 and 6.2 GPa were collected by a four-circle X-ray diffractometer. The bulk modulus determined by the Birch-Murnaghan equation-of-state is K_{0T}=154(2)GPa (assuming K'=4). The axial compressibilities of this sample are β_a=2.02(8)×10^{-3} GPa^{-1}, β_b=1.42(5)×10^{-3} GPa^{-1} and β_c=2.25(4)×10^{-3} GPa^{-1}. The results of structure refinement at each pressure with anisotropic displacement parameters at ambient pressure and with isotropic displacement parameter at high pressures yielded *R* values of 2.66, 5.61, 5.43 and 5.91%, respectively. The mean Al-O bond distance was significantly decreased by compression. The inverse relationships of variation against temperature and pressure are observed for both the unit cell parameters and bond distances.

Introduction

Topaz [$Al_2SiO_4(OH, F)_2$] is one of the major hydrous minerals. It is known that the physical properties (Ribbe and Rosenberg, 1971), symmetry (Akizuki et al., 1979) and thermodynamic properties (Barton, 1982a; 1982b) of topaz was controlled by the OH content. In natural samples, it had been known that substitution of F by OH in topaz occured only to a limited extent [OH/(OH+F) < ~30%](e.g. Ribbe and Rosenberg, 1971). The restriction of OH-content had been considered to be caused by H-H repulsion when H atoms located at the forbidden region (e.g. Parise et al., 1980; Barton, 1982a). However, Abbott (1990) suggested from energy calculation that an OH end-member of topaz would be possible, when the hydrogen bonding was stabilized. This suggestion was confirmed by Wunder et al. (1993) who synthesized the OH end-member of topaz during their high pressure experiment at 7.0 GPa in the system Al_2O_3-SiO_2-H_2O.

Recently, Zhang et al. (2002) recognized OH-rich topaz (X_{OH}=0.55) in thick kyanite quartzites from ultrahigh-pressure belts of the Sule terrane, China. They pointed out that the variation of OH substitution for F in topaz depended on their environments. Therefore, it is expected that the crystallization temperature and pressure conditions control OH content in topaz. As the structures of both natural topaz and topaz-OH had been analyzed only at room temperature and ambient pressure, it is highly desired to study the structure of this mineral at high temperature and pressure. The present study analyzed the crystal structure of natural topaz by single crystal X-ray diffraction method under high pressure and high temperature.

Experimental

Colorless single crystal and powdered samples of natural topaz from Gilgit division, Pakistan were used in this study. Chemical composition was determined by electron probe micro analyzer (EPMA: JEOL, JXA-8800M) and gave the formula $Al_{2.01}Si_{1.00}O_4F_{1.57}(OH)_{0.43}$. Anomalous optical property often reported by Akizuki et al. (1979) was not observed by optical microscopy.

K. Komatsu, komatsu@ganko.tohoku.ac.jp Corresponding author
T. Kuribayashi, t-kuri@mail.tains.tohoku.ac.jp
Y. Kudoh, ykudoh@mail.tains.tohoku.ac.jp

X-ray diffraction measurements at elevated temperatures

The unit cell parameters at 298K, 423K, 573K, 723K, 873K, 1023K and 1173K and X-ray diffraction intensities data at 298K, 573K, 873K and 1173K were collected by an imaging plate (IP) X-ray diffractometer equipped with rotating anode (MoKα, 50kV, 80mA) and a U-shaped resistance heater (Huber: High temperature attachment Type231). The heating temperature was calibrated on melting points of three standard materials ($NaNO_3$: 580K, NaCl: 1074K, Au: 1335K). The unit cell parameters at high temperature and α-β phase transition (846K) of quartz (Fig. 1) were also used to check the measured temperature of the experiment. The relationship between set point temperature (T_x) and sample temperature (T_y) was described by the following quadratic polynomial equation,

$$T_y = 255.88252 - 1.52902\,T_x + 0.00756\,T_x^2 - 7.61826\times10^{-6}\,T_x^3 + 2.6034\times10^{-10}\,T_x^4 .$$

The X-ray diffractions at high temperatures were measured after heating with a rate of 10K/min. and keeping for 3 hours at desired temperature.

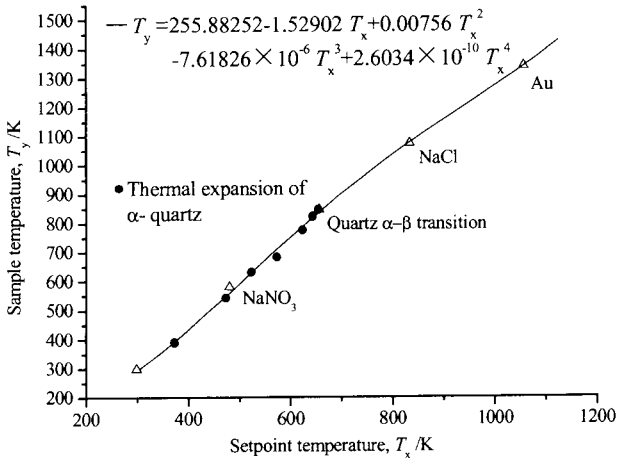

Figure 1. Temperature calibration by several melting points of standard materials and thermal expansion of quartz.

The powdered sample in fused silica capillary (ϕ 500μm) was used for the determination of the unit cell parameters at ambient and high temperatures. The obtained Debye rings were treated for one dimensional integration by a powder X-ray diffraction pattern refinement program using IP (PIP: Fujihisa, unpublished). The unit cell parameters obtained by least-squares fit are given in Table 1a. The specimen used for the collection of X-ray diffraction intensities at several temperatures was a single crystal (sample no. Pax08; size: 250 ×200 ×200μm^3) placed in a silica capillary (ϕ 300μm). The distance from IP to the sample was 80mm. The intensities of higher angle reflections were inaccurate, because the diffracted X-ray beams of higher angle were oblique angles with IP. Therefore, the maximum 2θ of the obtained reflections used for refinement were limited under 55° at room temperature and 45° at high temperature. Approximately 800 reflections in the above range of 2θ were measured. A total of 195-347 symmetry-independent reflections ($I_o \geq 2\sigma I_o$) were obtained by averaging the symmetry-equivalent intensities in Laue group *mmm*. Intensities were corrected for the Lorentz and polarization factors. The structures were refined in the space group *Pbnm* using a software package, CrystalStructure ver. 2.0 (Rigaku/MSC). Atomic coordinates and isotropic displacement parameters reported by Belokoneva et al. (1992) were used for initial data in the refinements. Spherical absorption correction was applied, and the Larson r^* secondary extinction parameter (Larson, 1970) was refined. Weighting schemes were based on w=1 (unit weight). Details on the intensity collection and structure refinements are given in Table 2a.

X-ray diffraction measurements at high pressures

The unit cell parameters under pressures up to 6.8 GPa and X-ray diffraction intensity data under pressures, 0.0001, 3.7, 5.1 and 6.2 GPa, were collected by a four-circle X-ray diffractometer with graphite monochromatized MoKα radiation (50kV, 30mA). Two single crystal specimens (sample no. Pax02; size: 80 × 80 ×40μm^3 and sample no. Pax05; size: 50 ×50 × 50μm^3) were used.

The modified Merill-Bassett-type diamond anvil pressure cell (Kudoh and Takeda, 1986) was used. A 0.25mm thick stainless steel (SUS301) plate was used as gasket material. A 16:3:1 mixture of methanol, ethanol and water were used as a fluid pressure medium. The pressure was calibrated by the ruby fluorescence method (Mao et al., 1986). The unit cell parameters obtained using 24 reflections in an angular region of 2θ =11° - 45° are given in Table 1b. Approximately 1100 reflections in a sphere accessible with the diamond anvil cell were measured, and a total of 221-330 symmetry-independent reflections ($I_o \geq 2\sigma I_o$) were obtained. The structures were refined in the space group *Pbnm* using the program SHELX97 (Sheldrick 1997). Weighting schemes were based on the following function:

$$w = 1 / [\ \sigma^2(F_o^2) + (aP)^2 + bP\ ],$$
where P is $[\ 2F_c^2 + \mathrm{Max}(F_o^2, 0)\ ] / 3$.

The use of this combination of F_o^2 and F_c^2 was shown by Wilson (1976) to reduce statistical bias. Other set up for intensity collections and structure refinements are summarized in Table 2b.

Results and discussion

Thermal expansion coefficients along crystal axes and of volume

Variations of the unit cell parameters and volume with temperature are shown in Figure 2a. The thermal expansion coefficients along crystal axes up to 1173K are α_a=6.4(7)×10^{-6}K^{-1}, α_b=5.5(6) ×10^{-6}K^{-1}, α_c=8.1(6) ×10^{-6}K^{-1} and α_V =2.0(1) ×10^{-5}K^{-1}. The ratio of the axial thermal expansion coefficients α_a: α_b: α_c is 0.79:0.68:1, showing significant anisotropy which is concordant with the presence of the perfect {001} cleavage of topaz. The expansion along the direction normal to the staking layer of closest packing of anion, b axis, was the smallest of the three principal axes.

Effect of temperature on the crystal structure

The results of structure refinement of Pax08 at 298K, 573K, 873K and 1173K with anisotropic atomic displacement parameters yielded R values of 2.48, 2.60, 2.56 and 2.70%, respectively. Although these R values was significantly low, it is necessary to consider the possibilities that the data obtained using flat IP such as R-axisIV^{++} have a systematic error by neglecting higher angle reflections. We compared the structural parameters of Pax08 at 298K and 0.0001 GPa to those of Pax02 at the same conditions. The atomic positions of Pax08 approximately equaled to those of Pax02, but the anisotropic displacement parameters showed significant difference exceeding the experimental errors (Tables 3a and 3b). Therefore, the numerical values of atomic positions obtained from IP are reliable, but those of the anisotropic displacement parameters are less reliable.

Table 1a. Unit cell parameters and volume at several temperatures and thermal expansion coefficients

Sample	T/K	a/Å	b/Å	c/Å	V/Å^3
Pax08	298	4.6489(24)	8.7935(39)	8.3957(39)	343.22(28)
	423	4.6561(20)	8.8056(33)	8.3989(38)	344.35(25)
	573	4.6593(23)	8.8121(36)	8.4171(36)	345.59(27)
	723	4.6640(23)	8.8173(36)	8.4255(36)	346.48(26)
	873	4.6680(25)	8.8244(39)	8.4340(39)	347.41(29)
	1023	4.6705(24)	8.8289(37)	8.4416(37)	348.09(28)
	1173	4.6774(25)	8.8405(39)	8.4554(39)	349.63(29)
The thermal expansion coefficient		α_a ×10^{-6}/K^{-1} 6.4(7)	α_b ×10^{-6}/K^{-1} 5.5(6)	α_c ×10^{-6}/K^{-1} 8.1(6)	α_V ×10^{-5}/K^{-1} 2.0(1)

Table 1b. Unit cell parameters, unit cell volume, the axial compressibility and bulk modulus

Sample	P/GPa	a/Å	b/Å	c/Å	V/Å^3
Pax02	0.0001	4.6500(9)	8.7996(17)	8.3902(14)	343.32(11)
	2.0	4.6346(18)	8.7792(23)	8.3519(15)	338.46(14)
	3.7	4.6193(20)	8.7579(25)	8.3174(17)	335.13(16)
	4.5	4.6124(28)	8.7431(34)	8.3023(23)	333.46(21)
Pax05	0.0001	4.6539(3)	8.8063(15)	8.3940(12)	342.63(8)
	1.4	4.6415(11)	8.7925(30)	8.3652(13)	340.01(14)
	2.3	4.6288(8)	8.7754(23)	8.3437(10)	337.56(11)
	3.2	4.6214(9)	8.7612(23)	8.3296(10)	335.90(11)
	3.9	4.6156(10)	8.7564(26)	8.3157(12)	334.73(13)
	5.1	4.6047(10)	8.7423(25)	8.2932(11)	332.50(12)
	5.9	4.5956(8)	8.7324(22)	8.2829(10)	331.06(11)
	6.2	4.5949(11)	8.7252(29)	8.2730(14)	330.34(14)
	6.8	4.5877(10)	8.7203(26)	8.2640(11)	329.28(12)
The axial compressibility and bulk modulus		β_a ×10^{-3} /GPa^{-1} 2.02(8)	β_b ×10^{-3} /GPa^{-1} 1.42(5)	β_c×10^{-3} /GPa^{-1} 2.25(4)	K /GPa 154(2)

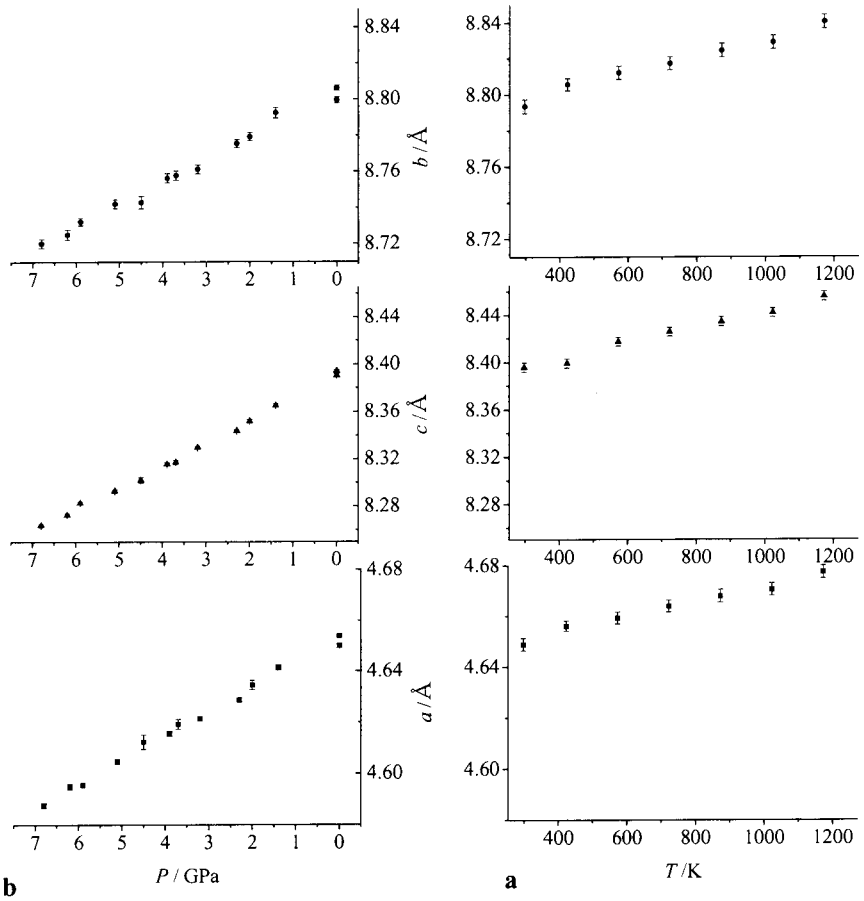

Figure 2. a Unit cell parameters at several temperatures. **b** Unit cell parameters at several pressures.

Table 2a. Several parameters of structure refinement at high temperature measurement

Sample	Pax08			
T /K	298	573	873	1173
$2\theta_{max}$	55	45	45	45
No. of reflections	347	217	195	213
No. of parameters	47	47	47	47
Para./refl. ratio	7.38	4.62	4.15	4.53
R^* (%)	2.48	2.60	2.56	2.70
wR† (%)	2.74	3.05	2.57	3.00
Goodness-of-fit	1.18	0.908	0.839	0.873
Ext. coef.	616.1	441.5	403.4	617.5

*$R=\Sigma||F_o|-|F_c|| / \Sigma|F_o|$
†$wR=\{\Sigma[w(F_o^2-F_c^2)^2] / \Sigma[w(F_o^2)^2]\}^{1/2}$, where $w = 1$

Table 2b. Several parameters of structure refinement at high pressure measurement

Sample	Pax02		Pax05		
P /GPa	0.0001	3.7	0.0001	5.1	6.2
$2\theta_{max}$	80	60	60	60	60
No. of reflections	610	247	330	224	221
No. of parameters	48	23	48	23	23
Para./refl. ratio	12.71	10.74	6.88	9.74	9.61
R (%)	3.15	5.61	2.66	5.43	5.91
wR† (%)	6.11	10.77	5.84	10.56	11.41
Goodness-of-fit	1.099	1.065	1.082	1.030	1.215
Ext. coef.	0.0850	0.0650	0.1930	0.1550	0.0240

*$R=\Sigma||F_o|-|F_c|| / \Sigma|F_o|$
†$wR=\{\Sigma[w(F_o^2-F_c^2)^2] / \Sigma[w(F_o^2)^2]\}^{1/2}$, where $w = 1 / [\ \sigma^2(F_o^2) + (aP)^2 + bP\ ]$, $P = [\ 2F_c^2 + \mathrm{Max}(F_o^2, 0)\ ] / 3$.

Table 3a. Atomic coordinates and atomic displacement parameters at several temperatures

Sample	T/K	Atom	x/a	y/b	z/c	U_{eq}	U_{11}	U_{22}	U_{33}	U_{23}	U_{13}	U_{12}
Pax08	298	Al	0.90358(15)	0.13102(8)	0.08240(9)	0.0031(3)	0.0038(4)	0.0036(5)	0.0023(4)	-0.0001(3)	0.0001(3)	0.0002(2)
		Si	0.6022(2)	0.05945(11)	0.75	0.0022(4)	0.0041(5)	0.0028(5)	0.0010(5)	0	0	0.0002(3)
		O1	0.7043(5)	0.0320(3)	0.25	0.0046(8)	0.0058(12)	0.0055(13)	0.0031(13)	0	0	-0.0008(9)
		O2	0.0434(5)	0.2564(3)	0.25	0.0046(7)	0.006(1)	0.0052(12)	0.0031(11)	0	0	0.0000(9)
		O3	0.2110(4)	0.9893(2)	0.0923(2)	0.0041(5)	0.0054(8)	0.0034(9)	0.0042(8)	-0.0000(7)	-0.0006(7)	0.0008(6)
		F	0.5981(3)	0.25265(18)	0.05741(17)	0.0065(4)	0.0084(7)	0.0070(7)	0.0052(7)	0.0001(6)	-0.0008(6)	0.0019(5)
	573	Al	0.9030(3)	0.13124(14)	0.08268(14)	0.0069(6)	0.007(1)	0.0052(9)	0.0095(9)	-0.0000(6)	0.0002(6)	-0.0003(6)
		Si	0.6027(4)	0.05953(19)	0.75	0.0048(6)	0.006(1)	0.0039(11)	0.0046(11)	0	0	-0.0004(7)
		O1	0.7027(9)	0.0325(5)	0.25	0.0074(11)	0.011(2)	0.006(2)	0.008(2)	0	0	-0.0023(19)
		O2	0.0433(9)	0.2565(5)	0.25	0.0089(11)	0.008(2)	0.009(2)	0.011(2)	0	0	-0.001(2)
		O3	0.2103(6)	0.9886(3)	0.0929(3)	0.0075(10)	0.0075(17)	0.0053(17)	0.0132(17)	-0.0012(14)	-0.0020(13)	-0.0020(14)
		F	0.5992(5)	0.2528(3)	0.0566(3)	0.0124(8)	0.0119(14)	0.0096(14)	0.0184(15)	0.0008(12)	-0.0011(11)	0.0036(11)
	873	Al	0.9029(3)	0.13122(13)	0.08245(16)	0.0095(6)	0.0105(11)	0.0081(11)	0.0104(9)	0.0001(6)	-0.0003(6)	0.0009(6)
		Si	0.6027(4)	0.05946(18)	0.75	0.0070(7)	0.0091(12)	0.0059(12)	0.006(1)	0	0	0.0002(8)
		O1	0.7013(9)	0.0324(5)	0.25	0.0091(14)	0.013(2)	0.005(2)	0.011(2)	0	0	-0.0013(19)
		O2	0.0428(9)	0.2565(5)	0.25	0.0111(12)	0.009(2)	0.015(2)	0.011(2)	0	0	-0.002(2)
		O3	0.2096(6)	0.9886(3)	0.0931(3)	0.0107(10)	0.0099(17)	0.0098(18)	0.0139(16)	0.0004(14)	-0.0026(14)	0.0016(15)
		F	0.5995(5)	0.2529(3)	0.0563(3)	0.0169(9)	0.0207(17)	0.0139(15)	0.0202(14)	0.0010(14)	-0.0028(11)	0.0063(11)
	1173	Al	0.9024(3)	0.13119(15)	0.08266(15)	0.0151(6)	0.0181(11)	0.013(1)	0.0144(9)	0.0004(6)	-0.0001(6)	0.0011(6)
		Si	0.6036(4)	0.0595(2)	0.75	0.0117(7)	0.0152(11)	0.0099(11)	0.0106(11)	0	0	-0.0002(8)
		O1	0.7007(9)	0.0325(5)	0.25	0.0159(14)	0.022(2)	0.012(2)	0.016(3)	0	0	-0.003(2)
		O2	0.043(1)	0.2568(5)	0.25	0.0172(11)	0.018(2)	0.020(2)	0.015(2)	0	0	-0.003(2)
		O3	0.2095(6)	0.9882(3)	0.0938(3)	0.0157(10)	0.0184(19)	0.0143(18)	0.0164(17)	0.0007(13)	-0.0038(13)	0.0030(14)
		F	0.5999(5)	0.2531(3)	0.0556(3)	0.0238(8)	0.0284(17)	0.0223(15)	0.0264(15)	0.0028(13)	-0.0038(12)	0.0095(12)

Table 3b. Atomic coordinates and atomic displacement parameters at several pressures

Sample	P /GPa	Atom	x/a	y/b	z/c	U_{eq} or U_{iso}†	U_{11}	U_{22}	U_{33}	U_{23}	U_{13}	U_{12}
Pax02	0.0001	Al	0.90349(11)	0.13102(5)	0.08251(6)	0.00405(12)	0.00463(21)	0.00386(21)	0.00365(24)	0.00006(15)	-0.00027(16)	0.00006(15)
		Si	0.60227(14)	0.05945(7)	0.75	0.00337(13)	0.00353(25)	0.00360(28)	0.00297(27)	0	0	0.00029(20)
		O1	0.70424(35)	0.03187(19)	0.25	0.00494(27)	0.00425(62)	0.00628(74)	0.00429(70)	0	0	-0.00112(49)
		O2	0.04427(34)	0.25624(19)	0.25	0.00453(28)	0.00633(69)	0.00345(70)	0.00382(72)	0	0	-0.00110(42)
		O3	0.21055(24)	0.98925(13)	0.09277(14)	0.00489(20)	0.00554(46)	0.00493(51)	0.00419(45)	0.00003(37)	-0.00068(36)	0.00069(32)
		F	0.59826(21)	0.25256(11)	0.05722(12)	0.00706(25)	0.00704(44)	0.00713(48)	0.00702(48)	0.00115(28)	-0.00102(33)	0.00256(36)
	3.7	Al	0.90376(39)	0.13131(20)	0.08173(13)	0.00777(49)						
		Si	0.60110(46)	0.05964(26)	0.75	0.00576(48)						
		O1	0.70907(115)	0.02782(72)	0.25	0.00833(92)						
		O2	0.04344(109)	0.25583(65)	0.25	0.00696(105)						
		O3	0.21260(79)	0.99085(43)	0.09179(28)	0.00717(70)						
		F	0.59515(69)	0.25297(37)	0.06036(23)	0.00892(66)						
Pax05	0.0001	Al	0.90365(15)	0.13097(8)	0.08254(8)	0.00496(25)	0.00558(41)	0.00509(38)	0.00420(38)	-0.00021(25)	-0.00093(20)	0.00047(26)
		Si	0.60211(20)	0.05946(10)	0.75	0.00422(27)	0.00491(47)	0.00439(45)	0.00335(43)	0	0	0.00019(35)
		O1	0.70441(50)	0.03160(27)	0.25	0.00479(48)	0.00459(101)	0.00663(110)	0.00314(93)	0	0	-0.00016(98)
		O2	0.04361(51)	0.25602(26)	0.25	0.00509(49)	0.00661(114)	0.00584(107)	0.00284(98)	0	0	-0.00096(94)
		O3	0.21055(36)	0.98924(19)	0.09230(18)	0.00520(37)	0.00527(81)	0.00577(80)	0.00457(64)	-0.00004(55)	0.00051(66)	0.00027(62)
		F	0.59831(28)	0.25263(16)	0.05729(16)	0.00875(47)	0.00884(81)	0.00944(75)	0.00797(71)	0.00107(52)	-0.00025(58)	0.00176(63)
	5.1	Al	0.90377(33)	0.13116(28)	0.08196(16)	0.00571(47)						
		Si	0.59945(42)	0.06005(39)	0.75	0.00543(50)						
		O1	0.70937(111)	0.02983(101)	0.25	0.00865(104)						
		O2	0.04748(102)	0.25579(104)	0.25	0.00830(112)						
		O3	0.21561(75)	0.99287(67)	0.09134(37)	0.00706(73)						
		F	0.59389(61)	0.25179(53)	0.06063(31)	0.00825(66)						
	6.2	Al	0.90320(25)	0.13079(26)	0.08201(14)	0.00497(49)						
		Si	0.60033(35)	0.05929(35)	0.75	0.00496(48)						
		O1	0.71152(96)	0.03050(91)	0.25	0.00672(100)						
		O2	0.04673(89)	0.25545(84)	0.25	0.00545(99)						
		O3	0.21519(72)	0.99245(68)	0.09080(33)	0.00762(74)						
		F	0.59181(42)	0.25210(48)	0.06173(30)	0.00754(67)						

† Equivalent and isotropic atomic displacement parameters were applied to ambient pressure and high pressure data, respectively.

Table 4a. Selected bond distances at several temperatures

Sample		Pax08				
T/K		298	573	873	1173	$\alpha\times10^{-6}$/K^{-1}
Al	-O1	1.897(2)	1.900(3)	1.908(3)	1.912(3)	10(2)
	-O2	1.902(2)	1.905(3)	1.909(3)	1.914(3)	7(2)
	-O3	1.898(2)	1.908(3)	1.908(3)	1.915(3)	9(2)
	-O3	1.885(2)	1.892(3)	1.893(3)	1.901(3)	9(2)
	-F	1.790(2)	1.788(3)	1.791(3)	1.793(3)	2(3)
	-F	1.801(2)	1.804(3)	1.805(3)	1.807(3)	4(3)
Al	-F $_{ave.}$	1.796	1.796	1.798	1.800	3
Al	-O $_{ave.}$	1.896	1.901	1.905	1.911	9
Al	-anion $_{ave.}$	1.862	1.866	1.869	1.874	7
Si	-O1	1.636(3)	1.638(5)	1.635(5)	1.639(5)	1(5)
	-O2	1.642(3)	1.645(5)	1.648(4)	1.649(5)	5(5)
	-O3	1.640(2)	1.639(3)	1.643(3)	1.639(3)	0(3)
Si-O $_{ave.}$		1.639	1.641	1.642	1.642	2
F	-O1	3.081(3)	3.095(4)	3.101(4)	3.110(5)	10(2)
	-O2	3.044(3)	3.059(5)	3.070(5)	3.082(5)	14(3)
	-F	3.234(3)	3.255(5)	3.267(5)	3.287(6)	18(3)

Table 4b. Selected bond distances at several pressures

Sample		Pax02		Pax05			
P/GPa		0.0001	3.7	0.0001	5.1	6.2	$\beta\times10^{-4}$/GPa^{-1}
Al	-O1	1.896(1)	1.895(4)	1.898(2)	1.878(5)	1.864(5)	23(5)
	-O2	1.902(1)	1.888(4)	1.901(2)	1.889(6)	1.884(5)	12(4)
	-O3	1.898(1)	1.886(4)	1.899(2)	1.879(5)	1.875(5)	20(5)
	-O3	1.888(1)	1.875(4)	1.886(2)	1.882(5)	1.870(4)	15(5)
	-F	1.790(1)	1.789(4)	1.792(1)	1.783(4)	1.788(3)	5(4)
	-F	1.801(1)	1.790(3)	1.803(2)	1.792(4)	1.791(3)	10(4)
Al	-F $_{ave.}$	1.795	1.790	1.797	1.788	1.790	8
Al	-O $_{ave.}$	1.896	1.886	1.896	1.882	1.873	17
Al	-anion $_{ave.}$	1.896	1.886	1.896	1.882	1.873	17
Si	-O1	1.636(2)	1.625(6)	1.636(2)	1.625(7)	1.633(6)	8(7)
	-O2	1.644(2)	1.638(6)	1.648(3)	1.628(10)	1.635(9)	14(10)
	-O3	1.638(1)	1.633(3)	1.642(2)	1.634(4)	1.630(4)	9(4)
Si-O $_{ave.}$		1.639	1.632	1.642	1.629	1.633	10
F	-O1	3.081(3)	3.017(9)	3.081(4)	3.032(9)	3.024(7)	18(5)
	-O2	3.042(2)	2.997(5)	3.047(2)	2.966(5)	2.950(4)	50(3)
	-F	3.235(3)	3.155(7)	3.235(4)	3.141(12)	3.112(10)	60(6)

As shown in Table 4a, the mean distance of Al-O bond significantly increased, while those of Al-F bond and Si-O2 bond increased slightly only less than 1σ. Figure 3a also shows the results of calculation using the following equation determined by Downs et al. (1994) for the bond length correction between a cation and an anion held with a strong rigid bond.

$$R_{SRB}^{\ 2} = R_{OBS}^{\ 2} + \frac{3}{8\pi^2}[B_{iso}(A) - B_{iso}(C)]$$

where R_{SRB} is the length of the simple rigid bond, R_{OBS} is the observed bond length, and $B_{iso}(A)$ and $B_{iso}(C)$ are the isotropic temperature factors for the anions and cation, respectively. The mean distance of Si-O1 and Si-O3 bond remained almost constant. As shown in Table 5a, the volume of $Al_2O_4F_2$ octahedron and SiO_4 tetrahedron showed similar trend for the bond distance, that is, the thermal expansion coefficient of $Al_2O_4F_2$ octahedron increased significantly with temperature, while those of

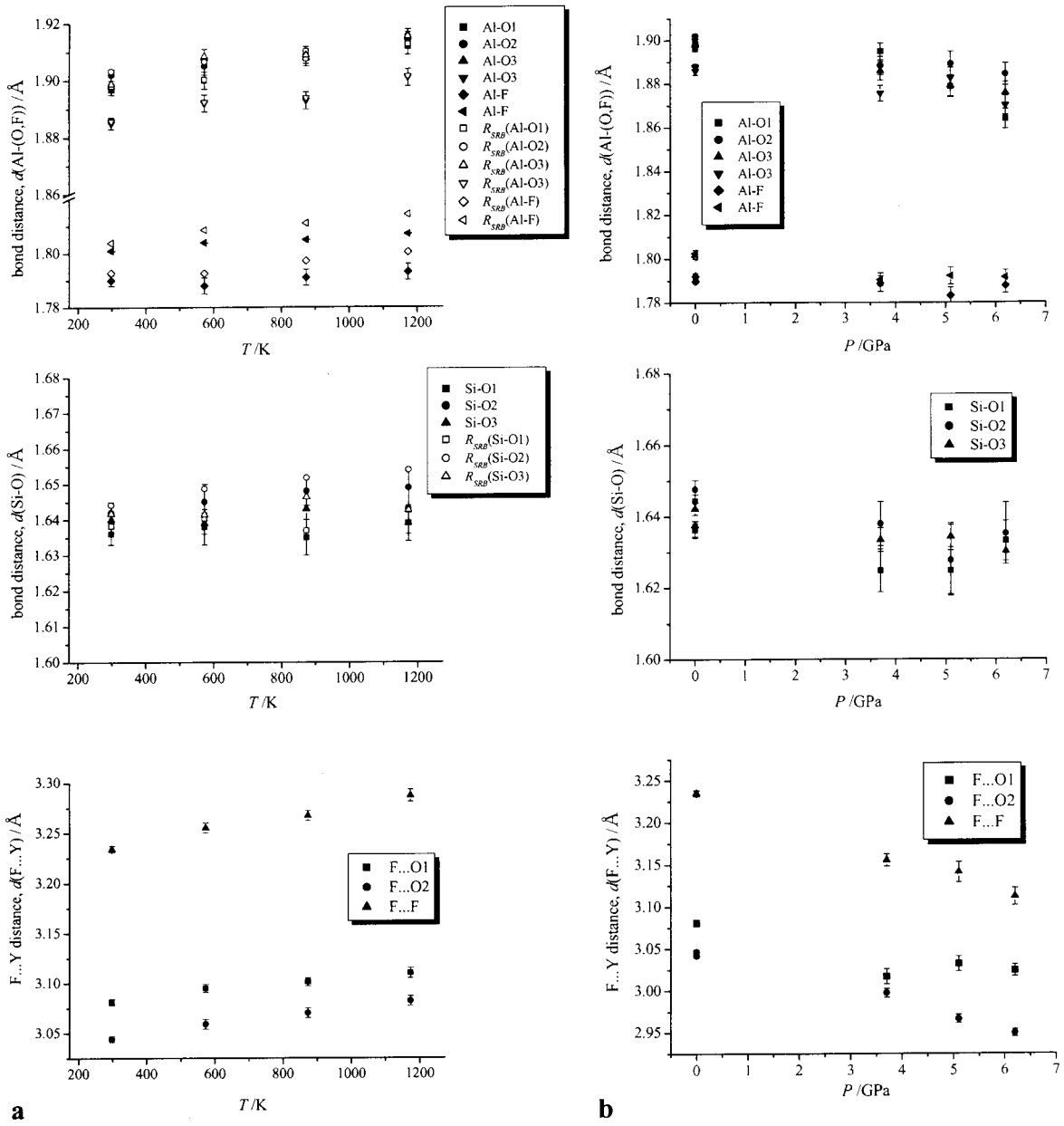

Figure 3. a The observed bond distances and the lengths of the simple rigid bond(R_{SRB}) at several temperatures. **b** Bond distances at several pressures.

SiO_4 tetrahedron remained almost constant. This result is consistent with the fact that the *c* axis, which passes through the layer without crossing Si-O bonds, was the most expansible direction. It should be noted that thermal expansion coefficients of F to anion distances (10-18 $\times 10^{-6}K^{-1}$) were larger than that of Al to anion distances (2-10 $\times 10^{-6}K^{-1}$) and Si-O bonds (0-5 $\times 10^{-6}K^{-1}$). The Al-O bond distances increased with increasing temperature while the Si-O bonds distances remained almost constant. This tendency appears also in the other aluminum silicate (Winter and Ghose, 1979), but the thermal response of the tetrahedral bond in low albite (Winter et al., 1977), in which many T-O bond distances decreased with increasing temperature, did not appear in topaz. Taken thermal vibration into consideration (Fig. 3a), the Si-O bonds slightly increased with temperature, but the difference between these values and the observed bond lengths was subtle. Therefore, as indicated by Winter and Ghose (1979), reduction in observed bond distances due to thermal vibration was greater in albite than in the other aluminum silicates.

Table 5a. Polyhedral volume and polyhedral thermal expansion coefficients

Sample	T /K	AlO_4F_2 octahedron V /Å^3	SiO_4 tetrahedron V /Å^3
Pax08	298	8.52	2.26
	573	8.58	2.26
	873	8.62	2.27
	1173	8.68	2.27
The polyhedral thermal expansion coefficient, $\alpha \times 10^{-5}$ /K^{-1}		2.0(1)	0.4(2)

Table 5b. Polyhedral volume and polyhedral bulk modulus

Sample	P /GPa	AlO_4F_2 octahedron V /Å^3	SiO_4 tetrahedron V /Å^3
Pax02	0.0001	8.53	2.26
	3.7	8.42	2.23
Pax05	0.0001	8.54	2.27
	5.1	8.38	2.22
	6.2	8.31	2.23
The polyhedral bulk modulus, K /GPa		251(19)	324(76)

Table 6a. Selected bond angles at several temperatures

Sample	Pax08			
T /K	298	573	873	1173
Al-O1-Al	95.8(1)	95.6(2)	95.5(2)	95.51(2)
Al-O2-Al	95.4(1)	95.4(2)	95.5(2)	95.26(2)
Al-O3-Al	97.0(1)	97.1(1)	97.1(1)	96.97(1)
Al-F-Al	144.5(1)	145.1(2)	145.3(2)	145.7(2)
O1-Al-O2	83.3(1)	83.4(1)	83.4(1)	83.53(1)
O3-Al-O3	83.1(1)	82.9(1)	82.9(1)	83.03(1)
F-Al-F	89.0(1)	89.0(1)	89.0(1)	88.90(1)
Al-Al-Al	113.86(6)	113.96(8)	113.91(8)	113.97(8)
O1-Si-O2	109.9(2)	109.9(2)	110.0(2)	109.84(2)
O1-Si-O3	109.5(1)	109.5(2)	109.6(2)	109.60(2)
O2-Si-O3	110.3(1)	110.2(2)	110.2(1)	110.19(2)
O3-Si-O3	107.4(2)	107.5(2)	107.3(2)	107.38(2)

Table 6b. Selected bond angles at several pressures

Sample	Pax02		Pax05		
P /GPa	0.0001	3.7	0.0001	5.1	6.2
Al-O1-Al	95.67(8)	95.25(26)	95.58(11)	95.79(33)	96.45(31)
Al-O2-Al	95.27(8)	95.69(28)	95.38(11)	95.10(37)	95.07(32)
Al-O3-Al	97.00(6)	96.96(16)	97.09(8)	96.65(18)	96.78(16)
Al-F-Al	144.67(6)	142.79(15)	144.63(9)	142.57(17)	141.93(16)
O1-Al-O2	83.52(6)	83.74(18)	83.50(8)	83.78(26)	83.48(18)
O3-Al-O3	83.00(6)	83.04(16)	82.91(8)	83.35(18)	83.22(16)
F-Al-F	88.95(3)	89.47(8)	88.94(4)	89.30(11)	89.27(10)
Al-Al-Al	113.87(5)	113.63(9)	113.87(7)	113.67(10)	113.65(9)
O1-Si-O2	109.97(9)	108.77(33)	109.83(13)	110.47(37)	110.00(30)
O1-Si-O3	109.54(6)	109.70(20)	109.56(8)	108.61(26)	108.87(24)
O2-Si-O3	110.20(6)	110.66(19)	110.20(8)	110.89(25)	110.62(22)
O3-Si-O3	107.34(9)	107.35(26)	107.44(12)	107.25(30)	107.80(30)

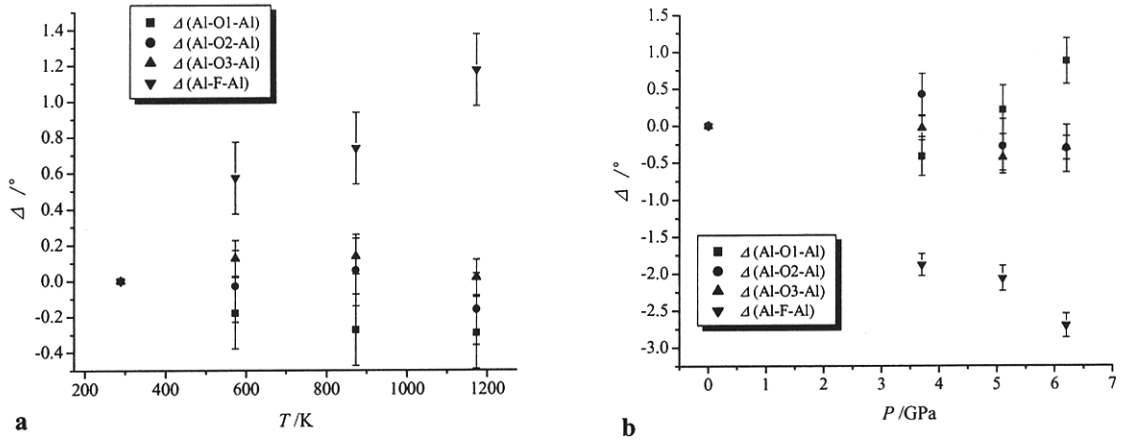

Figure 4. a Differences of bond angles from room temperature. **b** Differences of bond angles from ambient pressure.

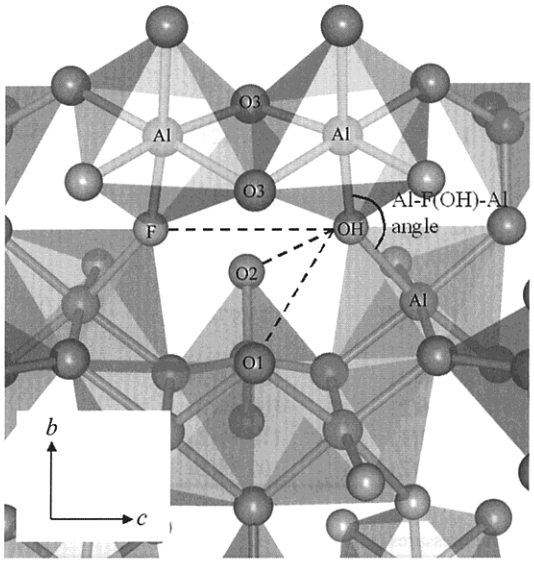

Figure 5. Schematic drawing of Al-F-Al bond angle's change.

Selected bond angles with temperature are listed in Table 6a, and those variations of bond angles from room temperature are shown in Figure 4a. The Al-F-Al bond angle increased with temperature from 144.5(1)° to 145.7(2)°, while other bond angles showed little change. As shown in Figure 5, if a fluorine-atom is apart from the neighboring fluorine-atom by heating, the Al-F-Al bond angle should increase. And so vice versa, the increase of the Al-F-Al bond angle is consistent with the most expansive F...F distances.

Isotropic atomic displacement parameter of fluorine-atom had the largest value of all atoms in topaz at room temperature and enhanced at high temperature. In addition, the largest principle axis of thermal ellipsoid of fluorine-atom was perpendicular to the plane defined by three Al-F-Al atoms as shown in Figure 6.

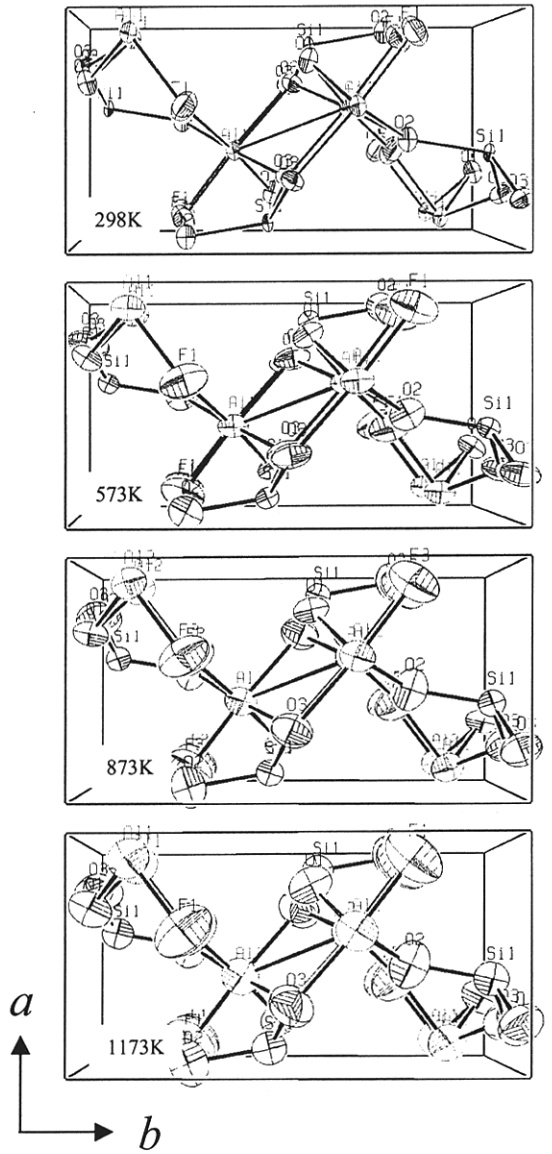

Figure 6. Displacement ellipsoids drawn with probability of 99% at elevated temperatures.

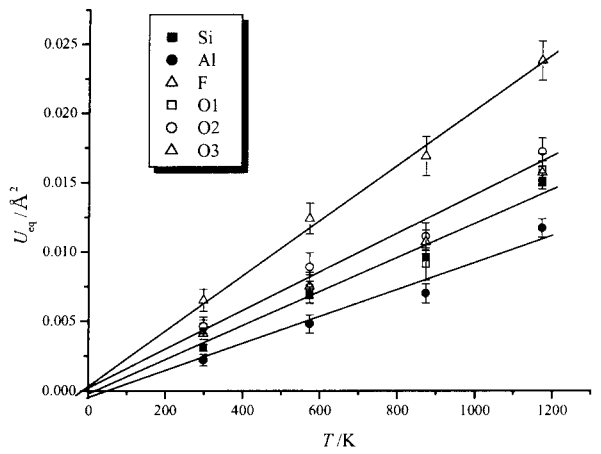

Figure 7. Temperature dependences of isotropic atomic displacement parameter.

In general, the large isotropic atomic displacement is attributed to thermal vibration and/or positional disorder. To distinguish the effect, the isotropic atomic displacements are plotted against temperature in Figure 7. When we extrapolated the isotropic atomic displacement of each atom to 0K, these values converged approximately to 0. Therefore, the large isotropic atomic displacement of fluorine-atom can be attributable to thermal vibration.

Compressibilities along crystal axes and isothermal bulk modulus

All three unit cell constants decreased with pressure (Fig. 2b). Accordingly, the bulk modulus determined by the Birch-Murnaghan equation-of-state up to 6.2GPa is K_{0T}=154(2) GPa (assuming K'=4). The ratio of the axial compressibilities are β_a=2.02(8)×10^{-3} GPa^{-1}, β_b=1.42(5)×10^{-3} GPa^{-1} and β_c=2.25(4)×10^{-3} GPa^{-1}. Axial compression ratios β_a: β_b: β_c is 0.90:0.63:1. These ratio with pressure was quantitatively similar to those with temperature (α_a: α_b: α_c = 0.79:0.68:1), that is, the variation of the unit cell parameters showed "inverse relationship" (Fig. 8), the term of which had been presented on some authors (e.g. Hazen and Finger, 1982; Hazen et al., 2000) on the relationship between thermal expansion and compression.

Haussühl (1993) determined elastic constants of topaz and several minerals using ultrasonic resonance of thick plates. The mean elastic stiffness of topaz, C=174.3 GPa, was greater than the isothermal bulk modulus obtained in the present study. The elastic stiffness tended to be larger than the isothermal bulk modulus at room temperature. Our result was in good agreement with the relationship between bulk modulus and molar volumes for the Al_2SiO_5 polymorphs obtained by previous authors (Yang et al., 1997b; Vaughan and Weidner, 1978; Ralph et al., 1984) as shown in Figure 9. The bulk modulus of topaz obtained by X-ray analysis in this study was consistent to the results of other aluminum silicates.

Topaz has the crankshaft-chain of AlO_4F_2 octahedra along the c axis. The Al_2SiO_5 polymorphs also have chains of AlO_6 octahedra, and especially in andalusite and sillimanite. These octahedra arrange along the c axis. However, the structure along the c-axis of andalusite and sillimanite was less compressible than along the a or b axes. These results seem different from our results. The most compressible direction was the c axis. The crankshaft-chain of topaz consists of a pair of edge-shared AlO_4F_2 octahedra and corner-shared linkage of those pairs. On the other hand, there are, in addition to the edge shared AlO_6 octahedra, double chains consisted of corner-shared SiO_4 tetrahedra and AlO_5 hexahedra in andalusite, or SiO_4 and AlO_4 tetrahedra in sillimanite as pointed out by Yang et al. (1997b). The crankshaft-chain of topaz would be more flexible than the chains of the Al_2SiO_5 polymorphs. The difference between linkage of the chains of topaz and those of the Al_2SiO_5 polymorphs would result from the difference of the most compressible directions.

Effect of pressure on the crystal structure

The results of structure refinement of Pax02 at 0.0001GPa and 3.6GPa, and Pax05 at 0.0001GPa, 5.1GPa and 6.2GPa, with anisotropic atomic displacement parameters at ambient pressure and with isotropic atomic displacement parameter at high pressures, yielded R values of 3.15, 5.61% for Pax02 and 2.66, 5.43, 5.91% for Pax05, respectively (Table. 2b). The obtained atomic coordinates and anisotropic atomic displacement parameters for Pax02 and Pax05 at several pressures are shown in Table 3b. Selected bond distances, polyhedral volumes and bond angles with pressure are shown in Tables 4b, 5b and 6b, respectively.

The structural variation with pressure was showing opposite trend to that with temperature. The mean Al-O distances significantly decreased with increasing pressure, while the mean Al-F distances and the mean Si-O slightly decreased. The cation-anion distances versus V/V_0 showed large variation in contrast to the unit cell parameters versus V/V_0 (Figs. 8 and 10). The systematic errors might be caused by the present of the blind region in reciprocal space inevitable in the

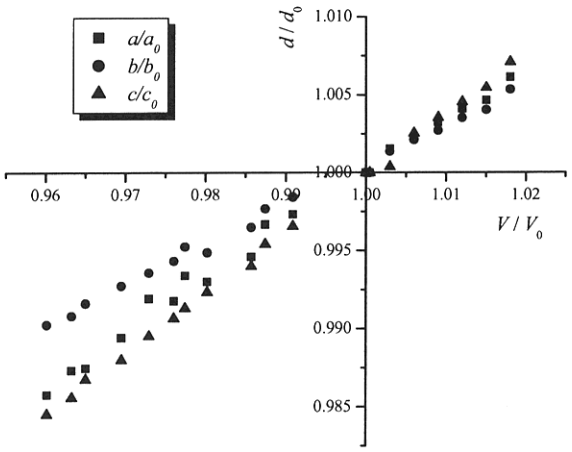

Figure 8. Unit cell parameters versus V/V_0.

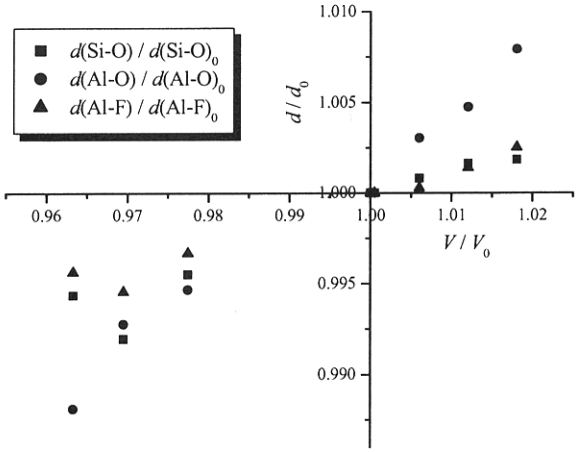

Figure 10. Cation-anion distances versus V/V_0.

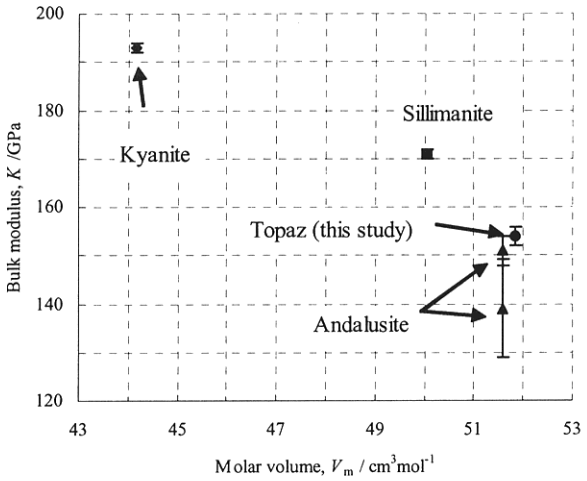

Figure 9. The relationship between the bulk modulus of several aluminum silicates and their molar volumes (modified by Yang et al., 1997a). Molar volume and the bulk modulus of topaz are 8.54 Å^3 and 251(19) GPa, respectively.

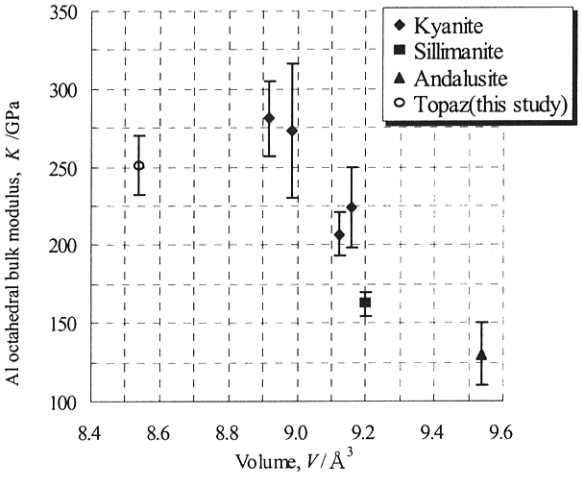

Figure 11. The bulk modulus-volume relationship for AlO_6 octahedra in the three Al_2SiO_5 polymorphs and AlO_4F_2 octahedra in topaz (modified by Yang et al., 1997a).

diamond anvil pressure cell and the different orientations for Pax02 and Pax05. The changes of polyhedral volumes was due to the variation of the bond distances. The AlO_4F_2 octahedral bulk modulus was 251(19) GPa. In contrast, the SiO_4 tetraheral bulk modulus was 324(76) GPa. The former seemed similar to the bulk modulus of AlO_6 octahedra in many structures, which agreed with the 235($\pm$ 10%)GPa reported by Hazen et al., (2000). However, the AlO_4F_2 octahedron did not behave in similar way with AlO_6 octahedron. Yang et al. (1997a) showed the relationship between the bulk modulus of the three Al_2SiO_5 polymorphs and their molar volumes, the bulk modulus-volume relationship for AlO_6 octahedra in kyanite and andalusite. As mentioned above, our result was in good agreement with the relationship between bulk modulus and molar volumes for the Al_2SiO_5 polymorphs (Fig. 9). On the other hand, our result of AlO_4F_2 octahedral bulk modulus differed from the relationship indicated by Yang et al. (1997a) (Fig. 11). This discrepancy came from the fact that the Al-F distances was shorter than the Al-O distances by ~0.1Å, and then the AlO_4F_2 octahedral volume was smaller than AlO_6 octahedral volume. AlO_4F_2 octahedral bulk modulus was consequently lager than AlO_6 octahedral bulk modulus. The substitution of F for O affected the

compression of aluminum polyhedral volume.

The variation of bond angles with pressure showed the opposite trend with temperature effect. The Al-F-Al bond angle decreased with pressure, while other bond angles were kept almost constant within 2σ (Fig. 4b). F...F distances seemed more compressible than the other distances for the opposite reason to the case of structure change with temperature. Substituting OH for F, the F...F distances, in other words OH...Y (Y=O or F) distances, could be considered as one of the candidate for hydrogen bond distances, because these distances would be shorter than 3.0Å at high pressure to about 7 GPa (Fig. 3b). The OH...O1, OH...O2 and OH...F distances of Pax05 at 6.2GPa are 3.024(7) Å, 2.950(4) Å and 3.112(10) Å, respectively. These values are similar to those of topaz-OH (OH...O1: 3.054Å, OH...O2: 2.961Å, OH...OH: 3.100Å) at ambient pressure determined by Northrup et al. (1994), and topaz-OH had been confirmed to form hydrogen bonds by infrared spectroscopy (Wunder et al., 1999).

From the present work, especially from bond-length and angle change around OH...Y at high pressures and at high temperatures, topaz-OH would be favored more than natural topaz at higher pressure conditions because of the formation of hydrogen bonding. As the nature of hydrogen bonding is not clear now at high pressures, spectroscopic work of hydrogen bonding in topaz at high pressure is desirable.

Conclusion

Thermal expansion and compression of topaz are controlled by those of Al-O bond distances which change significantly with temperatures and pressures. The structural variation with pressure is opposite to those with temperature, showing "inverse relationship". Several comparisons between topaz and Al_2SiO_5 polymorphs indicate that the linkage of chains of Al octahedra and the substitution of F for O affect thermal expansion and compression mechanism of topaz. The OH...Y distances, a candidate for the hydrogen bond, is more compressive than other atomic distances. This is provoked by the Al-F-Al bond angle which decreases with increasing pressure.

Acknowledgement

We thank H. Fujihisa for assistance in the installation of the pattern integration software PIP. Figure 5 was drawn with 3D visualization system VENUS developed by Dilanian and Izumi.

References

Abbott, R.N. Jr. (1990) Topaz: Energy calculations bearing on the location of hydrogen. The Canadian Mineralogist, 28, 827-834.

Akizuki M., Hampar, M.S. and Zussman, J. (1979) An explanation of anomalous optical properties of topaz. Mineralogical Magazine, 43, 237-241.

Barton, M.D. (1982a) The thermodynamic properties of topaz solid solution and some petrological applications. American Mineralogist, 67, 956-974.

Barton, M.D., Haselton, H.T. Jr., Hemingway, B.S., Kleppa, O.J. and Robie, R.A. (1982b) The thermodynamic properties of fluor-topaz. American Mineralogist, 67, 350-355.

Belokoneva, E.L., Smirnitskaya, Y.Y. and Tsirel'son, V.G. (1993) Electron density distribution in Topaz $Al_2[SiO_4](F,OH)_2$ as determination from high-precision X-ray diffracition data. Russian Jouranl of Inorganic Chemistry, 38-8, 1252-1256.

Downs, R.T., Hazen, R.M. and Finger, L.W. (1994) The high-pressure crystal chemistry of low albite and the origin of the pressure dependency of Al-Si ordering. American Mineralogist, 79, 1042-1052.

Finger, L.W., Hazen, R.M. and Hofmeister, A.M. (1986) High-pressure crystal chemistry of spinel ($MgAl_2O_4$) and magnetite (Fe_3O_4): Comparisons with silicate spinels. Physics and Chemistry of Minerals, 13, 215-220.

Haussühl, S. (1993) Thermoelastic properties of beryl, topaz, diaspore, sanidine and periclase. Zeitschrift für Kristallographie, 204, 67-76.

Hazen, R.M. and Finger, L.W. (1982) Comparative Crystal Chemistry: Temperature, Pressure, Composition and the Variation of Crystal Structure. John Wiley & Sons, New York.

Hazen, R.M., Downs, R.T. and Prewitt, C.T. (2000) Principles of comparative crystal chemistry. Reviews in Mineralogy, Vol 41. Mineralogical Society of America, Washington, DC.

Kudoh, Y. and Takeda, H. (1986) Single crystal X-ray diffraction study on the bond compressibility of fayalite, Fe_2SiO_4 and rutile, TiO_2 under high pressure, Physica, 139 and 140B, 333-336.

Larson, A.C. (1970) Crystallographic Computing (Ahmed, F.R. Ed.). Copenhagen, Munksgaard, 291-294.

Mao, H.K., Xu, J. and Bell, P.M. (1986) Calibration of the ruby pressure gauge to 800kbar under quasi-hydrostatic conditions. Journal of Geophysical Research, B91, 4673-4676.

Northrup, P.A., Leinenweber, K. and Parise J.P. (1994) The location of H in the high-pressure synthetic $Al_2SiO_4(OH)_2$ topaz analogue. American Mineralogist, 79, 401-404a.

Parise, J.B., Cuff, C. and Moore, F.H. (1980) A neutron diffraction study of topaz: evidence for lower symmetry. Mineralogical Magazine, 43, 943-944.

Ralph, R.L., Finger, L.W., Hazen, R.M. and Ghose, S. (1984) Compressibility and crystal structure of andalusite at high pressure. American Mineralogist, 69, 513-519.

Ribbe, P.H. and Gibbs, G.V. (1971) The crystal structure of topaz and

its relation to physical properties. American Mineralogist, 56, 24-30.

Ribbe, P.H. and Rosenberg, P.E. (1971) Optical and X-ray determinative methods for fluorine in topaz. American Mineralogist, 57, 168-187.

Sheldrick, G.M. (1997) SHELX-97. Program for crystal-structure refinement. University of Göttingen, Germany.

Sueno, S. (1983) Resistance heater systems for the high temperature single crystal X-ray diffraction experiments. Journal of the mineralogical society of Japan, 16(1), 5-11. (in Japanese)

Vaughan, M.T. and Weidner, D.J. (1988) The relationships of elasticity and crystal structure in andalusite and sillimanite. Physics and Chemistry of Minerals, 3, 133-144.

Wilson, A. J. C. (1976) Statistical bias in least-squares refinement. Acta Crystallographica, A32, 994 - 996.

Winter, J.K., Ghose, S. and Okamura, F.P. (1977) A high-temperature study of the thermal expansion and the anisotropy of the sodium atom in low albite. American Mineralogist, 62, 921-931.

Winter, J.K. and Ghose, S. (1979) Thermal expansion and high-temperature crystal chemistry of the Al_2SiO_5 polymorphs. American Mineralogist, 64, 573-586.

Wunder, B., Rubie, D.C., Ross, C.R. II, Medenbach, O., Seifert, F. and Schreyer, W. (1993) Synthesis, stability, and properties of $Al_2SiO_4(OH)_2$: a fully hydrated analogue of topaz. American Mineralogist, 78, 285-297.

Wunder, B., Andrut, M. and Wirth, R. (1999) High-pressure synthesis and properties of OH-rich topaz. Europian Jounal of Mineralogy, 11, 803-813.

Yang, H., Downs, R.T., Finger, L.W., Hazen, R.M. and Prewitt, C.T. (1997a) Compressibility and crystal structure of kyanite, Al_2SiO_5, at high pressure. American Mineralogist, 82, 467-474.

Yang, H., Hazen, R.M., Finger, L.W., Prewitt, C.T. and Downs, R.T. (1997b) Compressibility and crystal structure of sillimanite, Al_2SiO_5, at high pressure. Physics and Chemistry of Minerals, 25, 39-47.

Zhang, R.Y., Liou, J.G. and Shu, J.F. (2002) Hydroxyl-rich topaz in high-pressure and ultrahigh-pressure kyanite quartzites, with retrograde woodhouseite, from the Sulu terrane, eastern China American Mineralogist, 87, 445-453.

Manuscript received; 9 May, 2003
Manuscript accepted; 24 September, 2003